Relevance of host cell surface glycan structure for cell specificity of influenza A virus

Markus Kastner[1,*], Andreas Karner[1,2,*], Rong Zhu[1,*], Qiang Huang[3], Dandan Zhang[4], Jianping Liu[3], Andreas Geissner[5,6], Anne Sadewasser[7], Markus Lesch[8], Xenia Wörmann[8], Alexander Karlas[8], Peter Seeberger[5,6], Thorsten Wolff[7], Peter Hinterdorfer[1,2,§], Andreas Herrmann[9,§] and Christian Sieben[9,10,§]

[1] *Institute for Biophysics, Johannes Kepler University Linz, 4020 Linz, Austria*

[2] *Center for Advanced Bioanalysis GmbH, A-4020 Linz, Austria*

[3] *State Key Laboratory of Genetic Engineering, School of Life Sciences, Fudan University, Shanghai 200433, China*

[4] *Shanghai Supercomputer Center, Shanghai 201203, China*

[5] *Department for Biomolecular Systems, Max Planck Institute for Colloids and Interfaces, Potsdam, Germany*

[6] *Institute of Chemistry and Biochemistry, Free University, Berlin, Germany*

[7] *Div. of Influenza and other Respiratory Viruses, Robert Koch-Institute, 13353 Berlin, Germany*

[8] *Molecular Biology Department, Max Planck Institute for Infection Biology, 10117 Berlin, Germany*

[9] *Department of Biology, Molecular Biophysics, Humboldt Universität zu Berlin, 10115 Berlin, Germany*

[10] *Current address: Laboratory for Experimental Biophysics, School of Basic Sciences, École Polytechnique Fédérale de Lausanne (EPFL), 1015 Lausanne, Switzerland*

[*] These authors contributed equally to this work

[§] Corresponding authors:

christian.sieben@epfl.ch (C.S.)

andreas.herrmann@rz.hu-berlin.de (A.H.)

peter.hinterdorfer@jku.at (P. H.)

Abstract

Influenza A viruses (IAV) initiate infection *via* binding of the viral hemagglutinin (HA) to sialylated glycan receptors on host cells. HAs receptor specificity towards sialic acid (SA) is well studied and clearly critical for virus infection, but the contribution of the highly complex cellular plasma membrane to the cellular specificity remains elusive. In addition, some studies indicated that other host cell factors such as the epidermal growth factor receptor might contribute to the initial virus-cell contact and further downstream signaling[1].

Here we use two complementary methods, glycan arrays and single-virus force spectroscopy (SVFS) to compare influenza virus receptor specificity with actual host cell binding. Unexpectedly, our study reveals that HAs receptor binding preference does not necessarily reflect virus-cell specificity. We propose SVFS as a tool to elucidate the cell binding preference of IAV thereby including the complex environment of sialylated receptors within the plasma membrane of living cells.

1. Introduction

Influenza A viruses circulate in aquatic birds, their large natural host reservoir, but have also established stable lineages in various mammalian species such as pigs. Although animal influenza viruses are usually confined to their natural host species, they can cause zoonotic infections in humans on rare occasions[2]. Such trans-species transmissions can result in clinically severe or even fatal respiratory disease in humans as illustrated by the outbreaks of avian-origin H7N9 subtype viruses in China occurring since 2013[3]. Zoonotic transmission events can, in fact, largely influence the epidemiology of human influenza directly if the virus succeeds to spread among humans as was observed in 2009 for the pandemic swine-origin H1N1 strain (pdmH1N1)[4]. Although the genetic requirements for crossing the species barrier are still incompletely understood, it is accepted that interspecies transmission of influenza A viruses partially depends on the capability of viral hemagglutinin (HA) to recognize specific sialylated-glycan receptors on the host cell surface. In general, HA of avian viruses preferentially binds to α-2,3-linked sialic acid (SA) (avian-type receptor) [5] whereas HA of human-adapted strains strongly bind to terminal α-2,6-linked SA (human-type receptor) [5]. Several studies have determined that alterations in HA receptor binding specificity are a crucial step in host adaptation and interspecies transmission for several IAV subtypes [6, 7, 8]. However, it is not well established if those adaptive mutations (1) provide an actual advantage in virus-cell binding during entry, or (2) whether they are necessary to confer transmission (i.e. by evading decoy receptors lining the human airway mucus) or (3) to avoid triggering of innate immune signaling. Regarding the first point, several studies suggest a much higher complexity of virus–cell interaction beyond the level of HA–SA binding (for a

review see[9]). Consequently, it was hypothesized that human influenza viruses bind to a more structurally diverse set of SA linked carbohydrates than avian viruses which goes beyond the general preference of α-2,3 or α-2,6 linkage.

Currently, glycan arrays with libraries of synthesized glycan structures are widely utilized for the characterization of IAV glycan specificity. In particular, due to direct exposure of receptors on the array, sialic acid specificity can be studied with high precision on structural glycan properties. However, the cellular glycome has been recently studied for human and swine respiratory tract tissue, showing that its complexity might not be well represented by current glycan arrays [13, 14]. Indeed, influenza virus infection in the absence of sialic acid suggests other possible attachment factors involved in virus binding . Candidates molecules are C-type lectins (L-SIGN and DC-SIGN), which were found to participate in influenza virus attachment independent of SA specificity [12]. Hence, complementary approaches to directly assess viral receptor specificity within the complex environment of the cell surface are necessary to reach a more comprehensive understanding of the initial stage of virus infection. As we have recently shown, atomic force microscopy (AFM)-based single-virus force spectroscopy (SVFS) allows to measure the binding of individual IAV to living host cells at the molecular level [15, 16, 17]. In this type of analysis, intact influenza viruses are covalently attached to AFM cantilevers, which are then lowered on single living cells (Fig. 1). Cycles between cantilever-cell approach, cell binding and cantilever retraction, allow direct characterization of virus cell binding, while revealing kinetic and thermodynamic properties of the interactions [15, 16]. Thus, SVFS allows to investigate virus-cell binding in an experimental system that closely mimics the natural situation.

Here, by using a set of five different influenza A virus strains, we systematically address whether virus-cell specific binding patterns as determined by SVFS are reflected in their receptor specificity observed by glycan array analysis. Our data indicate that results obtained from *in vitro* glycan arrays may not be directly transferred to virus-cell binding. We suggest that host cell specificity does not solely depend on the sialic acid configuration of the cell surface, but is more complex and depends on the specific environment of the receptor and possibly involves additional attachment factors or co-receptors with yet unknown functional roles.

2. Results

Receptor specificity of influenza A virus strains studied by glycan arrays. To investigate and compare the SA receptor specificity of different virus strains, we performed an *in vitro* glycan array study utilizing a library of 15 glycans (Fig. 2). Regarding specific IAV receptors, our library included three α-2,3-linked (avian-type) SA conjugates as well as three α-2,6-linked (human-type) SA conjugates. The glycan number nine, sialyl-Lewis^X (SLe^X) has due to its fucosylation a different topology and was, although α-2,3-linked to SA, separated from the two groups shown on the left side in Fig. 2.

We found that the zoonotic AH1 strain and the pandemic H1N1 virus recognized all six SA conjugates with a preference for α-2,6-linked (human-type) receptors. Such a dual-binding behavior was already observed before for pdmH1N1 (A/California/04/2009 and A/Hamburg/5/2009). The receptor binding preference of the human H7N9 isolate

A/Anhui/1/2013 (AH1) is still under debate. It was shown that AH1 exhibits increased human receptor binding while still preferring avian receptors [20], others reported on the specificity for human-type receptors [21]. Interestingly, when we looked at the cumulative difference between the tested virus strains (Fig. S1), receptor specificity of AH1 and pdmH1N1 was most similar (i.e. the lowest difference).

FPV recognized all three avian-type conjugates, but bound only one human-type conjugate, which is in line with previous findings using glycan arrays [22].

We further tested H3N2/X31 as well as H1N1/WSN. H3N2/X31 carries the HA of the human pathogenic strain A/Aichi/68, which was also previously shown to prefer α-2,6-linked (human-type) receptors [23]. In line with that, we found that H3N2/X31 only recognized human-type SA conjugates on the glycan array. The lab-adapted H1N1/WSN was previously shown to prefer α-2,6-linked (human-type) receptors over α-2,3-linked SA on re-sialylated erythrocytes [24]. In our hands H1N1/WSN bound all six receptors with no obvious preference.

Its worth mentioning that among all glycans, we observed the strongest binding for pdmH1N1, H1N1/WSN and AH1 to the kinked, fucosylated glycan SLe^X (Fig. 1). SLe^X is well-known as an integrin receptor on leucocytes [25], but was also shown to be recognized by different IAV subtypes [26]. However, FPV was shown to bind only the sulfated form of SLe^X, which is in line with our findings [22].

Cell specificity of influenza A virus strains studied by SVFS. Next, we used SVFS to characterize virus binding to two different cell types: First, we studied living A549 cells, a model cell line derived from the lower human respiratory tract, expressing both major SA

receptor types on the cell surface as shown by lectin binding [15, 18]. Secondly, CHO cells lack an α-2,6-specific sialyltransferase and only express α-2,3-linked SA. Hence, we chose them as a comparative model for studying viral binding to cells displaying only avian-type receptors [15]. For SVFS, intact viruses were covalently attached to AFM cantilevers as previously reported (Fig. 1)[17]. Binding to cells was measured in a dynamic range of increasing loading rates, i.e. pulling velocities to determine the dissociation rate at zero force k_{off}. Unbinding events were recorded and analyzed to obtain the rupture force F as well as the effective spring constant k_{eff}, defined as the slope of the force-distance curve at rupture (Fig. 3a). From k_{eff}, the loading rate r (force per time) was calculated by multiplication with the retraction velocity v. Notably, we used an adapted data analysis procedure, which takes the variable local conditions of a living cell surface into account [27]. Briefly, although the loading rate r should be constant for a given pulling speed v, recent studies have shown that the heterogeneity of a living cell surface leads to a broad distribution of observed loading rates [27]. Hence, to account for this effect, our approach does not rely on binning of loading rates, but takes each individual force-distance curve into account (Fig. 3c). By fitting the force spectra to a single energy barrier model (Fig. 3c, d, see *Materials and Methods*), we obtained the thermodynamic properties of the interaction such as the dissociation rate k_{off}, and the separation of the receptor-bound state to the energy barrier x_u (summarized in table 1). The dissociation rate k_{off} and its reciprocal, the bond lifetime τ_{off}, provide information about the stability of the underlying virus-cell interaction. The results for all virus-cell interaction pairs are illustrated in Fig. 2d. For details, please see *Materials and Methods*.

Fig. 3b shows a typical rupture force histogram and the accompanying probability density

function (pdf) of the interaction between influenza AH1 and A549 cells with a binding probability of 29.7 % (v = 500 nm/sec). The pdf shows a single peak at ~23 pN indicating specific interaction (red curve in Fig. 3b). After cell surface SA deprivation by neuraminidase (NA) treatment, the binding probability was reduced to 5-13 % while the pdf peak position was unchanged (red curves and inset in Fig. 3b). This verifies the specificity of our measurement for receptor interaction. The binned histograms are shown for comparison along with the fitted pdf.

For AH1, we observed pronounced binding to both tested cell lines, with rupture forces, between 10 and 100 pN depending on the applied loading rate (Fig. 3c, d). However, we found an about 40 % reduced dissociation rate for A549 compared to CHO cells, indicating preferential binding of human-type cell surfaces. We confirm this binding preference of AH1 by measuring binding to living MDCK cells, which express, similar to A549 cells, both human-and avian-type receptors. We observed preferential binding to MDCK cells compared to CHO cells (Fig. S2). For FPV, we observed about three times lower dissociation rates compared to AH1, with preferential binding to A549 (see table 1). pdmH1N1 virus showed similar dissociation rates as FPV, but without pronounced cell type preference. H3N2/X31 as well as H1N1/WSN were already studied by SVFS in our previous study[15] but reanalyzed using the improved fitting procedure described above. The fitting values are reported in table 1. H3N2/X31 showed stronger attachment to CHO cells, while binding of H1N1/WSN to A549 and CHO cells was almost identical [15].

3. Discussion

Among other methods, solid-phase binding assays or glycan arrays represent a widely used state-of-the-art way to analyze HA receptor specificity [28]. The desired ligand is coupled to a flat surface and can either be probed with intact viruses [7, 8] or purified HA [19], which is then detected using antibody binding. This makes them a powerful tool to screen large glycan subsets. Choosing the right library is critical and since recent glycomics studies indicate a large heterogeneity of host cell-specific glycans, this choice is not easily made [14, Byrd-Leotis, 2014 #5]. Also, the presentation (i.e. orientation and density) of the glycan is critical [29], a factor that can be estimated by performing avidity studies along with the glycan array [30]. In our study, we have performed glycan array binding to evaluate the receptor specificity of various virus strains along with testing their cell specificity using SVFS. While our glycan array results are largely in line with previous findings, SVFS results, as summarized in table 1 and Fig. 4a, suggest that HA's preference for human or avian-type receptors does not necessarily correlate with expected binding patterns to cell lines modelling the surfaces of human or avian cells (see below). We compared the specificity of virus binding measured in a glycan array (i.e. receptor specificity) with that measured by SVFS (i.e. cell specificity). For pdmH1N1 and H1N1/WSN, we found that the SVFS data (for H1N1/WSN see [15]) are in good agreement with results obtained from glycan array binding as neither strain displayed strong preference for human or avian-type receptors or a particular cell model.

However, we observed contradicting preferences for H3N2/X31, AH1 and also for FPV. H3N2/X31 was found to preferentially bind avian-type cell surfaces, while only recognizing

α-2,6-linked (human-type) receptors on the glycan array. AH1, similarly to pdmH1N1, recognized both receptor types on the glycan array and showed good binding to all six presented specific glycans on the array, while SVFS indicated a preference for human-type cell surfaces. FPV recognized all three avian, but only one human-type receptor on the glycan array, while showing preferential binding to human-type cell surfaces in SFVS. However, binding to the recognized human-type receptors (receptor 3 in Fig. 1) was about 2-3 fold stronger compared to the avian-type receptors (receptor 5 in Fig. 1), which might explain the stronger binding to A549 cells. In conclusion, our results suggest that the HAs receptor preference as tested in glycan array binding may not be a good predictor for preferred binding to human-type over avian-type cell surfaces.

The findings described above raised the possibility that non-sialic acid receptors contribute to a larger than expected extent to virus cell binding. However, SVFS analyses of cells after pre-treatment with neuraminidase to remove sialic acid structures showed that the binding probability was strongly reduced, leaving the unbinding force unchanged (Fig. 2B). This indicates that the viruses indeed mainly bind to sialic acid of the cell surface, but that the local environment of the receptor or other cell surface molecules alters the macroscopic cell specificity leading to the observed differences. The stronger binding of AH1, pdmH1N1 and H1N1/WSN to fucosylated glycan SLe^X with α-2,3-linked to SA in comparison to the other α-2,3-linked (avian-type) SA of our glycan array is indicative for the relevance of the local environment. On the viral side, cumulating evidence suggests a role of the viral neuraminidase (NA) in contributing to cell binding via sialic acid [31]. In our SVFS measurements, NA was kept active and, hence, it cannot be excluded as a binding mediator, a

feature that could be tested in future experiments.

We also took a closer look at the thermodynamic properties of the virus cell interaction (table 1). Comparison of the transition state distance x_u revealed values around 2-10 Å for viruses binding to A549 cells (mean 5.8 Å). In contrast, on CHO cells, we found higher transition state distances between 2-13 Å (mean 8.1 Å). This interesting feature was also previously observed for IAV H3N2/X-31[15] and suggests a differently shaped energy barrier. Correlation of x_u and k_{off} revealed no apparent clustering of H1 or H7 viruses (Fig. 4A) indicating a dynamic interaction potentially involving multiple different receptor sites. However, some correlation can be observed suggesting that binding to human-type cell surfaces tends to result in lower bond energy and shorter unbinding distance. Indeed, x_u could be a possible parameter to explore structural differences underlying virus-cell specificity. The observed x_u values fall within the distance regime between receptor and its binding pocket. As an example, Fig. 4C shows snapshots of a force-distance molecular dynamics simulation between HA from influenza A H3N2/X31 and its human-type receptor (taken from [15]). The distance between the terminal SA and Asn137 (magenta), part of the critical loop 130, is shown and scales between 4-20 Å. The corresponding value pair for x_u and k_{off} is shown in Fig. 3B (green).

4. Conclusion

Recent glycomics approaches and the use of *ex vivo* tissue culture revealed new insights into the complexity of the living cell surface [13, 14]. Since sialic acid was first identified as an influenza virus attachment factor [32], many studies have focused on HA-SA binding. Although

this interaction is clearly important, not only infection of desialylated cells [11], but also the recent characterization of non-SA binding hemagglutinin encoded by a bat-derived H17N10 virus[33], and the discovery that 1918 pandemic virus unaffectedly binds to primary human airway cells even when its HA is engineered to bind exclusively to avian-type SA receptors [34] suggested that other molecular determinants within the plasma membrane are also critical in initiating influenza A virus infection. For characterizing virus specificity, we suggest a dual complementary approach: (1) *in vitro* binding assays with synthetic glycans to precisely identify the preference of HA (or NA) for a specific sialic acid structure and (2) SVFS as demonstrated here to unravel the cell specificity, modulated by the local environment of the living host cell. We have recently demonstrated this complementary approach for an adapted mutant of pdmH1N1 [17]. While glycan array analysis could not identify a switch in receptor preference, SVFS revealed that the adaptive mutation in HA strongly reduced the binding strength without changing the cell specificity. These binding properties are not accessible and might be hidden when only using *in vitro* specificity assays. The use of new methods such as SVFS [16] and *ex vivo* tissue culture in combination with global glycomics and proteomics approaches could help to identify essential components of the plasma membrane facilitating influenza virus cell interaction.

Materials and Methods

Cell and virus propagation. Chinese hamster ovary (CHO) cells and human alveolar A549 cells were grown in DMEM (PAA) supplemented with 1% penicillin/streptomycin and 10% FCS (PAA) in plastic petri dishes. For sialic acid digestion, we used neuraminidase (NA) from *Clostridium perfringens* (Sigma) solved in PBS buffer. The cells were treated for 10 min at 37° C with 1 U/mL NA. Influenza A viruses were grown on 10-day old chicken eggs and purified from allantoic fluid by gradient centrifugation through a 20-60 % (w/v) sucrose gradient. The A/Anhui/1/2013 strain was inactivated by UV irradiation before gradient centrifugation.

Glycan array. Glycan array preparation was performed as described previously [35, Wormann, 2016 #192]. Briefly, glycans containing a primary amino linker were dissolved at a concentration of 0.1 mM in printing buffer (50 mM sodium phosphate, pH 8.5) and printed on N-hydroxysuccinimide activated glass slides (CodeLink slides, Surmodics, Edina, MN, USA) using an S3 robotic microarray spotter (Scienion, Berlin, Germany). Slides were incubated overnight in a humidity saturated chamber and remaining reactive groups were quenched by incubating with 100 mM ethanolamine, 50 mM sodium phosphate at pH 9.0 for 1 h at room temperature. Slides were washed with water, dried by centrifugation and stored at 4 °C until use. Before loading, the array was washed with DPBS. Virus was diluted as indicated into sterile binding buffer containing 1% BSA, 0.05% Tween 20 (MERCK), $CaCl_2$ (492 µM) and $MgCl_2$ (901 µM) at pH 7.0. 30 µl of diluted virus were pipetted in each well and the array was incubated in a moist chamber for 24 h at 4 °C. Each well was then washed three times with washing buffer containing DPBS and 0.1% Tween 20 (DPBS-T). Subsequently, wells

were blocked with DPBS containing 1% BSA for 2 h at 4 °C and permeabilized using DPBS-T containing 0.3% Triton-X100. To stain the bound virus the array was incubated with a primary monoclonal antibody against the viral NP protein (1:1000, clone AA5H, AbD Serotec, Oxford, UK) at 4 °C overnight. Primary antibody was removed and wells were washed three times with DPBS-T. Secondary Cy3-coupled goat anti-mouse IgG (1:100, product-code: 115-165-146, Jackson ImmunoResearch Laboratories, West Grove, PA, USA) was added and incubated at RT for 1 h. The array was washed three times with DPBS-T and dipped into distilled water before scanning. Glycan array fluorescence images were obtained using a GenePix 4300A microarray scanner (Molecular Devices, Sunnyvale, CA, USA). Fluorescence intensities of spots were evaluated with GenePix Pro 7.2 (Molecular Devices).

AFM tip chemistry. Commercially available AFM cantilevers (MSCT, Bruker) were amine functionalized by using the room-temperature method for reaction with APTES [36]. A heterobifunctional PEG linker, acetal–PEG_{800}–NHS (N-hydroxysuccinimide) (Fig. 1B), was attached by incubating the tip for 1.5-2 h in 0.5 mL of chloroform containing 2 mg/mL acetal–PEG–NHS and 8µL triethylamine, resulting in acylation of surface-linked APTES by the NHS group. The terminal acetal group was converted into an amine-reactive aldehyde by incubation in 1% citric acid as described previously [36]. After rinsing with water for 3 times, once with ethanol and drying under a stream of nitrogen, the tips were incubated in a mixture of 19-25 µL of approximately 0.6-1.6 mg/mL influenza A virus in PBS (without Ca^{++}) and 1-2 µL of 1 M $NaCNBH_3$ (freshly prepared by dissolving 32 mg of solid $NaCNBH_3$ in 500 µL of 10 mM NaOH) for 60 min. The tips were then washed in 3mL PBS for 3 times and stored in PBS at 4 °C. All other chemicals and reagents were purchased from different

commercial sources in the highest purity grade available.

SVFS measurement. As illustrated in Fig.1, AFM-based force spectroscopy was performed with an Agilent 5500 AFM. The Petri dish with cells was mounted with the AFM, which was put on the optical microscope through a specially designed XY stage. Before force measurements, the cantilever with a nominal spring constant of 10 pN/m functionalized with influenza A virus was incubated in 5 mg/mL BSA for 30 min in order to minimize the nonspecific interaction between the cantilever tip and the cell surface. Measurements were performed in PBS buffer at room temperature. After the cantilever tip approached to the cell surface, force distance curves were repeatedly measured with Z-scanning range of 2 µm, cycle duration of 0.5-8 s, 500 data points per curve, and typical force limit of about 40-70 pN. The spring constants of the cantilevers were determined by using the thermal noise method [37].

Fitting of SVFS data. Similar to single molecule force spectroscopy (SMFS), also in SVFS studies, several hundred force distance cycles are recorded in a dynamic range of increasing loading rates under identical conditions. For each of these force curves showing unbinding events, the unbinding force Fi and the effective spring constant k_{eff} (slope at rupture) were determined. The loading rates r were determined by multiplying the pulling velocity v with the effective spring constant k_{eff} (i.e. $r = v * k_{eff}$). Additionally, a rupture force probability density function (pdf) (Fig. 1d) was calculated and a Gaussian distribution was fitted to the main peak of the pdf. Subsequently, all unbinding events within $\mu \pm \sigma$ of the fit have been selected to create a loading rate dependence scatter plot (Fig. 1c-f) for further calculations of k_{off} and x_u.

342 Generally, the loading rate r is constant for a fixed pulling speed, which implies, that the
343 effective spring constant k_{eff} does not vary significantly. However, for force spectroscopy
344 measurements on live cells it is known, that k_{eff} could show a broadened distribution
345 caused by local variations of the spring constant of the cell surface, leading to a convolution
346 of the rupture force distribution and further influences the calculations for the dissociation
347 rate constant, k_{off}, and the separation of the receptor-bound state to the energy barrier, x_u.
348 To circumvent this influence, we applied a maximum likelihood routine to fit the SVFS data
349 to the Evans-model [27], in order to obtain k_{off} and x_u (Table 1).

350 Accordingly to the single energy barrier binding model, the probability p that the complex
351 breaks at a certain force, F, is given as [38]:

352 $$p(F) = \frac{k_{off}}{r} exp\left[\frac{F_{xu}}{k_B T} - \frac{k_{off} k_B T}{r x_u}\left(exp\frac{F x_u}{k_B T} - 1\right)\right] \quad (3)$$

353 The parameters x_u and k_{off} were determined by applying a maximum likelihood approach,
354 in which the negative log likelihood *nll* was minimized by modifying k_{off} and x_u, with p
355 based on Equation (3) defined in the single barrier model [38]:

356 $$nll = -\sum_t \log p(k_{off}, x_u, F_t, r_t) \quad (4)$$

357

358 **Acknowledgments**

359 This work was supported in part by the grants from the Hi-tech Research and Development
360 Program of China (2008AA02Z311), the Shanghai Natural Science Foundation
361 (13ZR1402400), the Shanghai Leading Academic Discipline Project (B111). The work was
362 further supported by the German Ministry of Research and Education (BMBF) (e:Bio
363 ViroSign) as well as the German Research Foundation (DFG) (SFB 765). R.Z. and P.H. were

supported by Austrian Research Fund SFB-F35.

Additional information

Supplementary information is available. Correspondence and requests for materials should be addressed to C.S., A.H. or P.H.

Competing financial interests

The authors declare no competing financial interests.

Table 1 | Dissociation rate k_{off}, separation from the energy barrier x_u, and average bond lifetime τ_{off} obtained by fitting the SVFS data to a single energy barrier binding model as described in Methods (see also Fig. 2D).

Cell (receptor type)	x_u (Å)	k_{off} (s^{-1})	τ_{off} (s)
Virus AH1 (H7N9)			
CHO (*avian-like*)	13.2 ± 0.016	1.17 ± 0.001	0.85
A549 (*human-like*)	9.24 ± 0.006	0.69 ± 0.0008	1.43
Virus FPV (H7N1)			
CHO (*avian-like*)	2.40± 0.004	0.33 ± 0.001	3.03
A549 (*human-like*)	5.74 ± 0.016	0.24 ± 0.001	4.15
Virus pdmH1N1			
CHO (*avian-like*)	12.5± 0.004	0.19 ± 0.001	5.20
A549 (*human-like*)	5.2 ± 0.016	0.2 ± 0.001	5.00
Virus X31 (H3N2)			
CHO (*avian-like*)	9.54 ± 0.18	0.66 ± 0.05	1.51
A549 (*human-like*)	6.42 ± 0.09	1.27 ± 0.07	0.78
Virus WSN (H1N1)			
CHO (*avian-like*)	2.77 ± 0.04	0.62 ± 0.04	1.61
A549 (human-*like*)	2.67 ± 0.04	0.85 ± 0.05	1.18

412 **Figure legends:**

413

414 **Figure 1 | Schematic diagram of the SVFS experimental setup using atomic force**
415 **microscopy (AFM). (A)** General principle of AFM-based SVFS. Cells grow in a plastic
416 culture dish that is attached to three step motors that allow movement with high accuracy.
417 The cantilever acts as a Hookean spring and hence bending can be translated into applied
418 force. The force-induced deflection of the cantilever is measured by pointing a laser on the
419 back of the cantilever while detecting the reflection on a quadrant photo diode (QPD). **(B)**
420 For SVFS, influenza A virions are covalently attached to the cantilever using an
421 acetal-PEG_{800}-NHS crosslinker [39]. (**C**) The cantilever is lowered on a single cell until
422 touching the cell surface. The combination with light microscopy, allows identification of the
423 cantilever with its pyramidal cantilever tip (**C**, inset shows a graphical illustration) and
424 thereby precise positioning. Subsequently, the cantilever is retracted at a defined velocity *v*.
425 In case of an interaction, the cantilever will bend towards the sample until the underlying
426 bond fails and the cantilever returns into the zero-force position (see also Fig. 2a).

427

428 **Figure 2 | Binding characteristics of the indicated viruses to sialic acid-conjugated**
429 **receptors quantified by glycan arrays**. Equal amounts of the indicated viruses were bound to
430 glycan arrays, spotted with 15 different sialic acids and printing buffer as negative control.
431 Staining of bound viruses was achieved using a NP-specific primary antibody and a
432 Cy3-coupled secondary antibody. The results represent the mean + SD for two independent

433 experiments.

434

435 **Figure 3 | SVFS measurements of H7 and pdmH1N1 viruses interacting with receptors**
436 **on living cells**. (**A**) Force trace of H7N9 AH1 virus-cell interactions measured by AFM-based
437 SVFS showing a characteristic single unbinding event. After treating the cells with
438 neuraminidase (NA), the binding probability was strongly decreased (see also inset in B),
439 causing a high number of force traces showing no interaction (inset in a). (**B**) Force histogram
440 (left Y axis) and overlaid force probability density function (pdf, right Y axis) of AH1
441 virus-A549 cell interaction before and after NA treatment. The observed force values were
442 found to be very similar, but the binding probability was strongly decreased (inset). (**C**)
443 Scatter plots showing unbinding force F plotted against the loading rate r of every individual
444 force curve from AH1 virus-A549 cell interaction. The red dotted line shows the fitting to the
445 single energy barrier model (see Methods). (**D**) Overview of the fittings used to determine
446 values for k_{off} and x_u (see table 1 and Methods) for all virus-cell combinations.

447

448 **Figure 4 | Comparing cell with receptor specificity and summary of the thermodynamic**
449 **parameters obtained from SVFS.** (**A**) To allow comparison between cell and receptor
450 specificity, we show results from SVFS (blue bars) as Δk_{off} (avian/human) as well as results
451 obtained from glycan arrays (red bars). The red bars indicating receptor specificity were
452 placed according to the number of recognized glycans as well as the strength of binding, as
453 discussed in section 2. (**B**) Correlation of k_{off} and x_u shows no apparent clustering for H7 (red)

or H1 (black) viruses indicating a very dynamic interaction (as shown in [15]) supposedly including various receptors. The distance to the transition state x_u provides a parameter to characterize the interacting cellular receptor as the distance between receptor and HA falls within this range. As an example, (**C**) shows snapshots of a force-probe molecular dynamics simulation between HA from influenza A/X31 (green) and a human-type receptor (red) (taken from [15]). The distance between the terminal SA and Asn137 (magenta) is shown and scales between 4-20 Å. The measured values for x_u and k_{off} for the corresponding virus-cell combination are shown in **B** (green).

Supplementary Figure Legends

Supplementary Figure S1. Cumulative receptor binding difference between H7N9/AH1 and the other on glycan arrays tested virus strains. For each glycan, the binding intensity was compared to the value of H7N9/AH1. The summed difference is shown for each virus strain revealing that H7N9/AH1 shares most similarities with pdmH1N1.

Supplementary Figure S2. SVFS dynamic force spectra of H7N9 AH1 interacting with single receptors on living MDCK cells. Scatter plot showing unbinding force F plotted against the loading rate r of every individual force curve. From those data, the values for k_{off} and x_u were determined to be 0.256 +/- 0.00169 s^{-1} and 6.160 +/- 0.0146 Å, respectively.

Supplementary Table S3. Comparing SVFS results obtained using two different fitting approaches. Loading rates LR can either be obtained by using the mean effective spring constant $\langle k_{eff} \rangle$ for each pulling velocity v ($LR = v * k_{eff}$) or, using a more adapted approach reported previously and now used in this study, calculated for each individual force-distance curve. Each fitting approach results in slightly different fitting parameters. Dissociation rate k_{off}, separation from the energy barrier x_u, and average bond lifetime τ_{off} obtained by fitting the SVFS data to a single energy barrier binding model.

References

1. Eierhoff T, Hrincius ER, Rescher U, Ludwig S, Ehrhardt C. The epidermal growth factor receptor (EGFR) promotes uptake of influenza A viruses (IAV) into host cells. *PLoS pathogens* 2010, **6**(9)**:** e1001099.

2. Reperant LA, Kuiken T, Osterhaus AD. Adaptive pathways of zoonotic influenza viruses: from exposure to establishment in humans. *Vaccine* 2012, **30**(30)**:** 4419-4434.

3. Gao R, Cao B, Hu Y, Feng Z, Wang D, Hu W, *et al.* Human infection with a novel avian-origin influenza A (H7N9) virus. *The New England journal of medicine* 2013, **368**(20)**:** 1888-1897.

4. Novel Swine-Origin Influenza AVIT, Dawood FS, Jain S, Finelli L, Shaw MW, Lindstrom S, *et al.* Emergence of a novel swine-origin influenza A (H1N1) virus in humans. *The New England journal of medicine* 2009, **360**(25)**:** 2605-2615.

5. Rogers GN, Paulson JC. Receptor determinants of human and animal influenza virus isolates: differences in receptor specificity of the H3 hemagglutinin based on species of origin. *Virology* 1983, **127**(2)**:** 361-373.

6. Herfst S, Schrauwen EJA, Linster M, Chutinimitkul S, de Wit E, Munster VJ, *et al.* Airborne Transmission of Influenza A/H5N1 Virus Between Ferrets. *Science* 2012, **336**(6088)**:** 1534-1541.

7. Imai M, Watanabe T, Hatta M, Das SC, Ozawa M, Shinya K, *et al.* Experimental adaptation of an influenza H5 HA confers respiratory droplet transmission to a reassortant H5 HA/H1N1 virus in ferrets. *Nature* 2012, **486**(7403)**:** 420-428.

8. Matrosovich M, Tuzikov A, Bovin N, Gambaryan A, Klimov A, Castrucci MR, *et al.* Early alterations of the receptor-binding properties of H1, H2, and H3 avian influenza virus hemagglutinins after their introduction into mammals. *Journal of virology* 2000, **74**(18)**:** 8502-8512.

9. Mair CM, Ludwig K, Herrmann A, Sieben C. Receptor binding and pH stability - how influenza A virus hemagglutinin affects host-specific virus infection. *Biochimica et biophysica acta* 2014, **1838**(4)**:** 1153-1168.

10. Stevens J, Blixt O, Glaser L, Taubenberger JK, Palese P, Paulson JC, *et al.* Glycan microarray analysis of the hemagglutinins from modern and pandemic influenza viruses reveals different receptor specificities. *J Mol Biol* 2006, **355**(5)**:** 1143-1155.

11. Stray SJ, Cummings RD, Air GM. Influenza virus infection of desialylated cells. *Glycobiology* 2000, **10**(7)**:** 649-658.

12. Londrigan SL, Turville SG, Tate MD, Deng YM, Brooks AG, Reading PC. N-linked glycosylation facilitates sialic acid-independent attachment and entry of influenza A viruses into cells expressing

DC-SIGN or L-SIGN. *Journal of virology* 2011, **85**(6)**:** 2990-3000.

13. Byrd-Leotis L, Liu R, Bradley KC, Lasanajak Y, Cummings SF, Song X*, et al.* Shotgun glycomics of pig lung identifies natural endogenous receptors for influenza viruses. *Proceedings of the National Academy of Sciences of the United States of America* 2014, **111**(22)**:** E2241-2250.

14. Walther T, Karamanska R, Chan RW, Chan MC, Jia N, Air G*, et al.* Glycomic analysis of human respiratory tract tissues and correlation with influenza virus infection. *PLoS pathogens* 2013, **9**(3)**:** e1003223.

15. Sieben C, Kappel C, Zhu R, Wozniak A, Rankl C, Hinterdorfer P*, et al.* Influenza virus binds its host cell using multiple dynamic interactions. *Proceedings of the National Academy of Sciences of the United States of America* 2012, **109**(34)**:** 13626-13631.

16. Herrmann A, Sieben C. Single-virus force spectroscopy unravels molecular details of virus infection. *Integrative biology : quantitative biosciences from nano to macro* 2015, **7**(6)**:** 620-632.

17. Wormann X, Lesch M, Welke RW, Okonechnikov K, Abdurishid M, Sieben C*, et al.* Genetic characterization of an adapted pandemic 2009 H1N1 influenza virus that reveals improved replication rates in human lung epithelial cells. *Virology* 2016, **492:** 118-129.

18. Schmier S, Mostafa A, Haarmann T, Bannert N, Ziebuhr J, Veljkovic V*, et al.* In Silico Prediction and Experimental Confirmation of HA Residues Conferring Enhanced Human Receptor Specificity of H5N1 Influenza A Viruses. *Scientific reports* 2015, **5:** 11434.

19. Xu R, McBride R, Nycholat CM, Paulson JC, Wilson IA. Structural characterization of the hemagglutinin receptor specificity from the 2009 H1N1 influenza pandemic. *Journal of virology* 2012, **86**(2)**:** 982-990.

20. Xiong X, Martin SR, Haire LF, Wharton SA, Daniels RS, Bennett MS*, et al.* Receptor binding by an H7N9 influenza virus from humans. *Nature* 2013, **499**(7459)**:** 496-499.

21. Watanabe T, Kiso M, Fukuyama S, Nakajima N, Imai M, Yamada S*, et al.* Characterization of H7N9 influenza A viruses isolated from humans. *Nature* 2013, **501**(7468)**:** 551-555.

22. Gambaryan AS, Matrosovich TY, Philipp J, Munster VJ, Fouchier RA, Cattoli G*, et al.* Receptor-binding profiles of H7 subtype influenza viruses in different host species. *Journal of virology* 2012, **86**(8)**:** 4370-4379.

23. Sauter NK, Hanson JE, Glick GD, Brown JH, Crowther RL, Park SJ*, et al.* Binding of influenza virus hemagglutinin to analogs of its cell-surface receptor, sialic acid: analysis by proton nuclear magnetic resonance spectroscopy and X-ray crystallography. *Biochemistry* 1992, **31**(40)**:** 9609-9621.

24. Leung HS, Li OT, Chan RW, Chan MC, Nicholls JM, Poon LL. Entry of influenza A Virus with a

alpha2,6-linked sialic acid binding preference requires host fibronectin. *Journal of virology* 2012, **86**(19)**:** 10704-10713.

25. Sperandio M, Gleissner CA, Ley K. Glycosylation in immune cell trafficking. *Immunological reviews* 2009, **230**(1)**:** 97-113.

26. Gambaryan AS, Tuzikov AB, Pazynina GV, Desheva JA, Bovin NV, Matrosovich MN*, et al.* 6-sulfo sialyl Lewis X is the common receptor determinant recognized by H5, H6, H7 and H9 influenza viruses of terrestrial poultry. *Virology journal* 2008, **5:** 85.

27. Wildling L, Rankl C, Haselgrubler T, Gruber HJ, Holy M, Newman AH*, et al.* Probing binding pocket of serotonin transporter by single molecular force spectroscopy on living cells. *The Journal of biological chemistry* 2012, **287**(1)**:** 105-113.

28. Stevens J, Blixt O, Paulson JC, Wilson IA. Glycan microarray technologies: tools to survey host specificity of influenza viruses. *Nature reviews Microbiology* 2006, **4**(11)**:** 857-864.

29. Papp I, Sieben C, Sisson AL, Kostka J, Bottcher C, Ludwig K*, et al.* Inhibition of influenza virus activity by multivalent glycoarchitectures with matched sizes. *Chembiochem : a European journal of chemical biology* 2011, **12**(6)**:** 887-895.

30. McBride R, Paulson JC, de Vries RP. A Miniaturized Glycan Microarray Assay for Assessing Avidity and Specificity of Influenza A Virus Hemagglutinins. *Journal of visualized experiments : JoVE* 2016(111).

31. Zhu XY, McBride R, Nycholat CM, Yu WL, Paulson JC, Wilson IA. Influenza Virus Neuraminidases with Reduced Enzymatic Activity That Avidly Bind Sialic Acid Receptors. *Journal of virology* 2012, **86**(24)**:** 13371-13383.

32. Gottschalk A. Chemistry of virus receptors. *The Viruses*, vol. 3. Academic Press, 1959.

33. Sun X, Shi Y, Lu X, He J, Gao F, Yan J*, et al.* Bat-derived influenza hemagglutinin H17 does not bind canonical avian or human receptors and most likely uses a unique entry mechanism. *Cell reports* 2013, **3**(3)**:** 769-778.

34. Davis AS, Chertow DS, Kindrachuk J, Qi L, Schwartzman LM, Suzich J*, et al.* 1918 Influenza receptor binding domain variants bind and replicate in primary human airway cells regardless of receptor specificity. *Virology* 2016, **493:** 238-246.

35. Pereira CL, Geissner A, Anish C, Seeberger PH. Chemical Synthesis Elucidates the Immunological Importance of a Pyruvate Modification in the Capsular Polysaccharide of Streptococcus pneumoniae Serotype 4. *Angewandte Chemie* 2015, **54**(34)**:** 10016-10019.

36. Rankl C, Kienberger F, Wildling L, Wruss J, Gruber HJ, Blaas D*, et al.* Multiple receptors involved in

human rhinovirus attachment to live cells. *Proceedings of the National Academy of Sciences of the United States of America* 2008, **105**(46)**:** 17778-17783.

37. Hinterdorfer P, Baumgartner W, Gruber HJ, Schilcher K, Schindler H. Detection and localization of individual antibody-antigen recognition events by atomic force microscopy. *Proceedings of the National Academy of Sciences of the United States of America* 1996, **93**(8)**:** 3477-3481.

38. Evans E, Ritchie K. Dynamic strength of molecular adhesion bonds. *Biophysical journal* 1997, **72**(4)**:** 1541-1555.

39. Wildling L, Unterauer B, Zhu R, Rupprecht A, Haselgrubler T, Rankl C*, et al.* Linking of sensor molecules with amino groups to amino-functionalized AFM tips. *Bioconjugate chemistry* 2011, **22**(6)**:** 1239-1248.

Figure 1

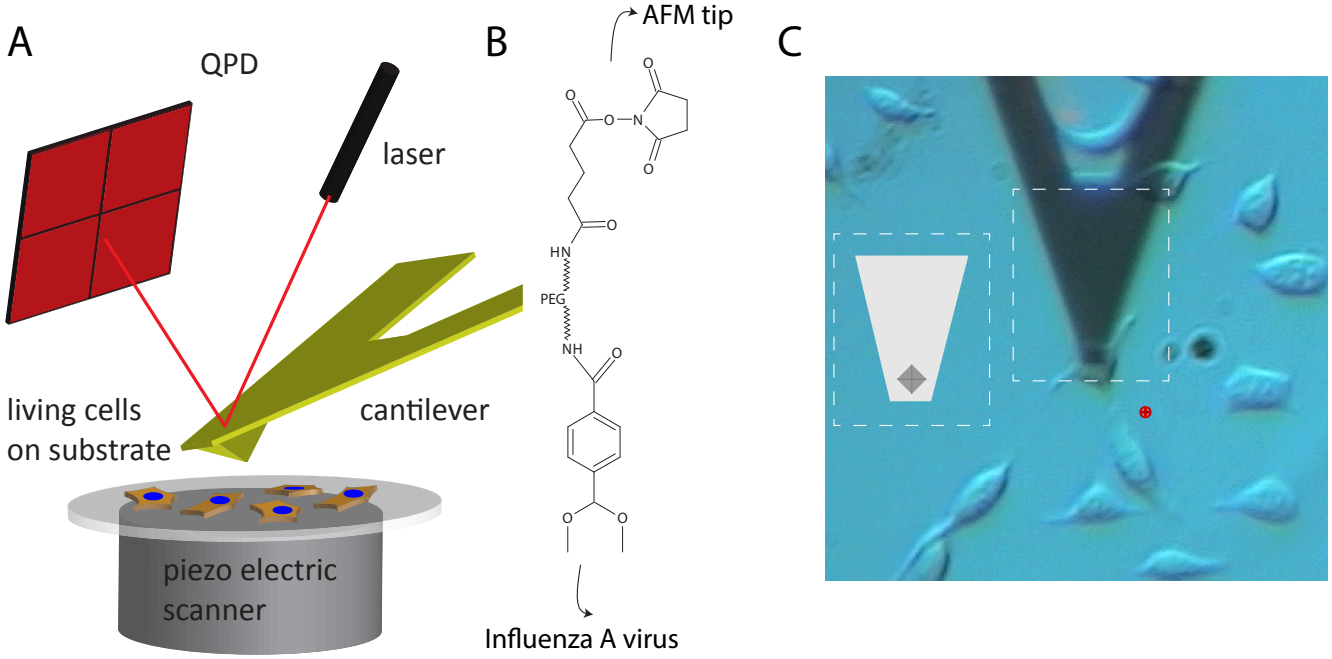

Figure 2

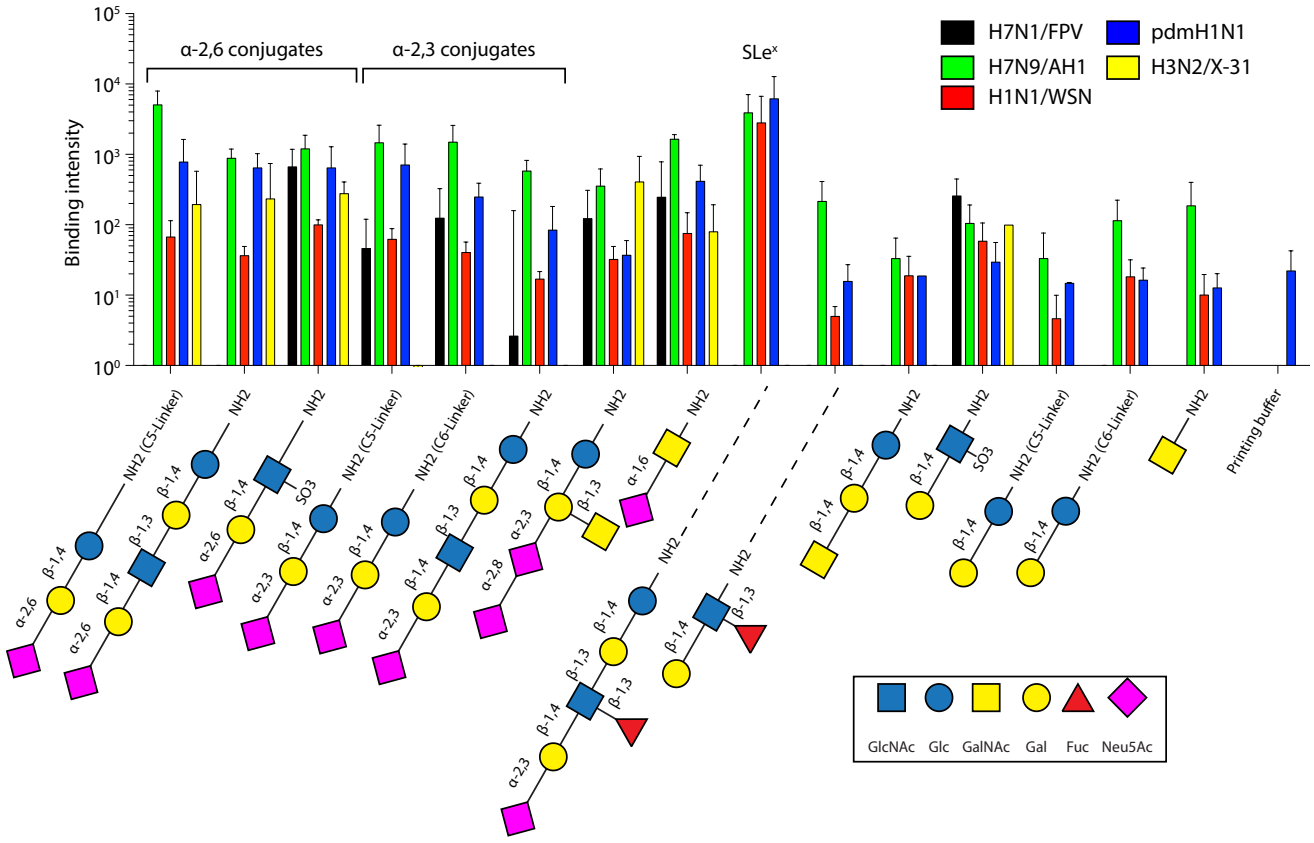

Figure 3

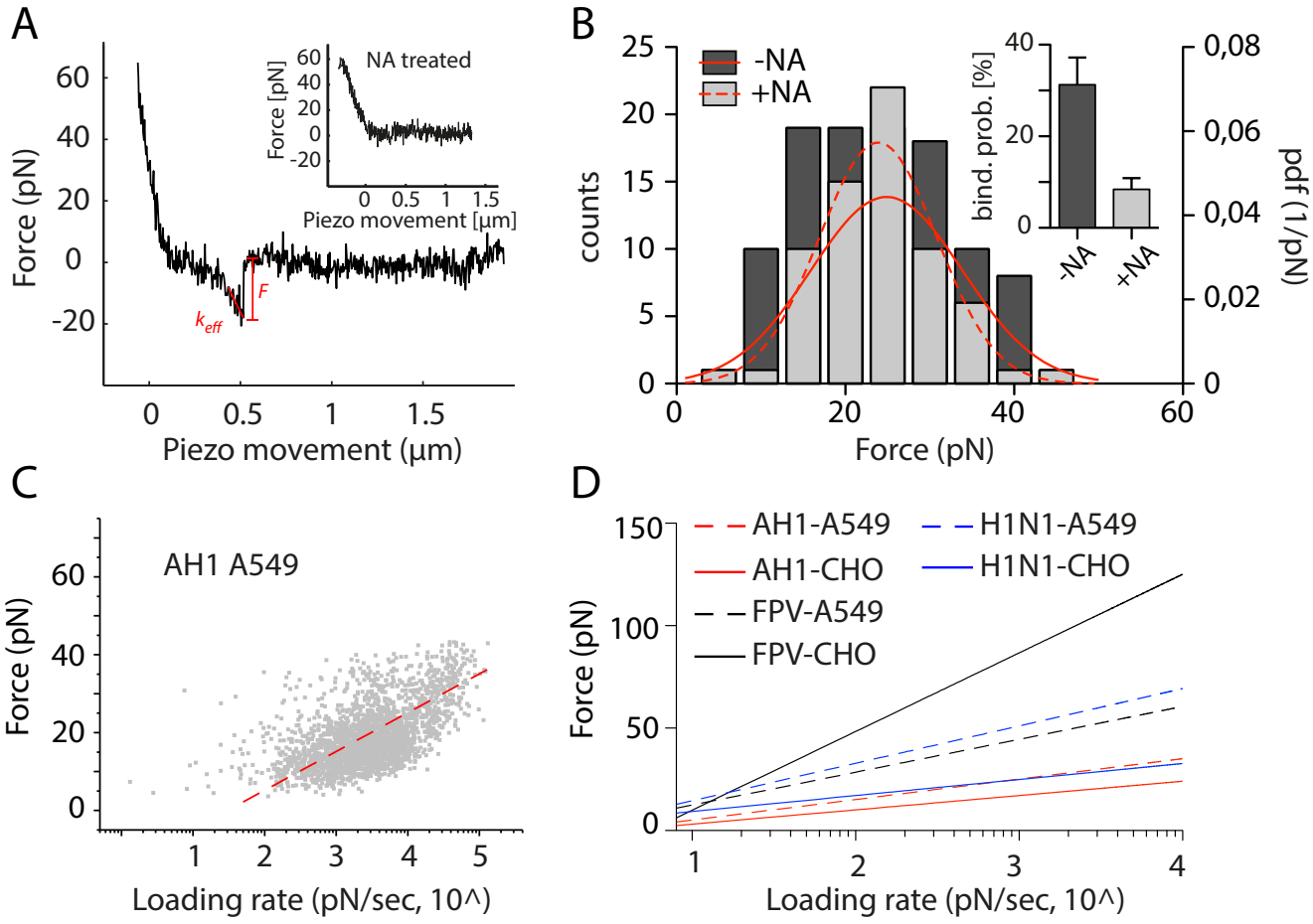

Figure 4

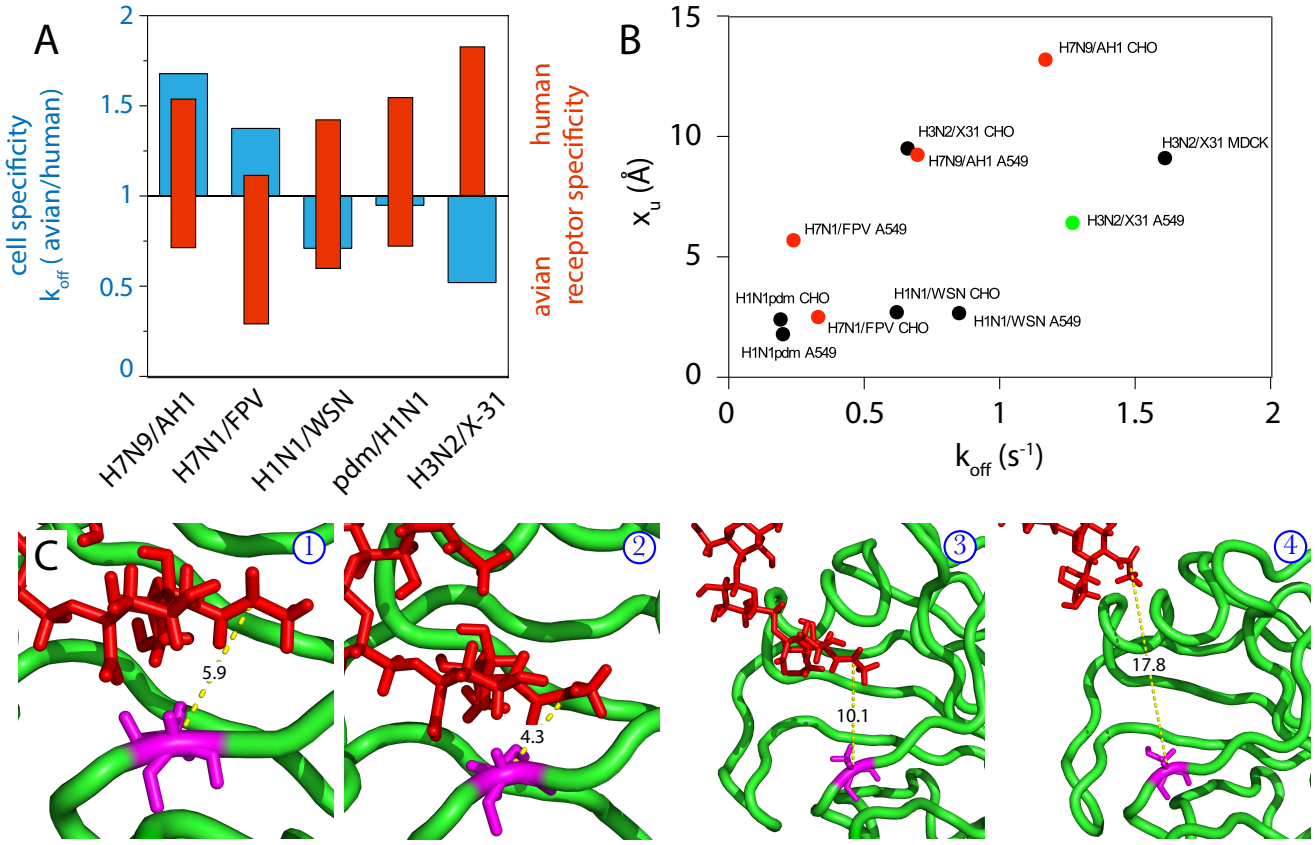

Supporting Information

Relevance of host cell surface glycan structure for cell specificity of influenza A virus

Markus Kastner[1,*], Andreas Karner[1,2,*], Rong Zhu[1,*], Qiang Huang[3], Dandan Zhang[4], Jianping Liu[3], Andreas Geissner[5,6], Anne Sadewasser[7], Markus Lesch[8], Xenia Wörmann[8], Alexander Karlas[8], Thorsten Wolff[7], Peter Hinterdorfer[1,2,§], Andreas Herrmann[9,§] and Christian Sieben[9,10,§]

[1] *Institute for Biophysics, Johannes Kepler University Linz, 4020 Linz, Austria*

[2] *Center for Advanced Bioanalysis GmbH, A-4020 Linz, Austria*

[3] *State Key Laboratory of Genetic Engineering, School of Life Sciences, Fudan University, Shanghai 200433, China*

[4] *Shanghai Supercomputer Center, Shanghai 201203, China*

[5] *Department for Biomolecular Systems, Max Planck Institute for Colloids and Interfaces, Potsdam, Germany*

[6] *Institute of Chemistry and Biochemistry, Free University, Berlin, Germany*

[7] *Div. of Influenza and other Respiratory Viruses, Robert Koch-Institute, 13353 Berlin, Germany*

[8] *Molecular Biology Department, Max Planck Institute for Infection Biology, 10117 Berlin, Germany*

[9] *Department of Biology, Molecular Biophysics, Humboldt University Berlin, 10115 Berlin, Germany*

[10] *Current address: Laboratory for Experimental Biophysics, School of Basic Sciences, École Polytechnique Fédérale de Lausanne (EPFL), 1015 Lausanne, Switzerland*

[*] These authors contributed equally to this work

[§] Corresponding authors:

christian.sieben@epfl.ch (C.S.)

andreas.herrmann@rz.hu-berlin.de (A.H.)

peter.hinterdorfer@jku.at (P. H.)

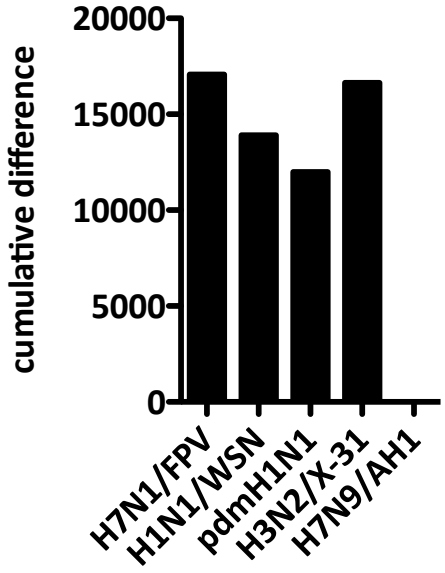

Supplementary Figure S1. Cumulative receptor binding difference between H7N9/AH1 and the other on glycan arrays tested virus strains. For each glycan, the binding intensity was compared to the value of H7N9/AH1. The summed difference is shown for each virus strain revealing that H7N9/AH1 shares most similarities with pdmH1N1.

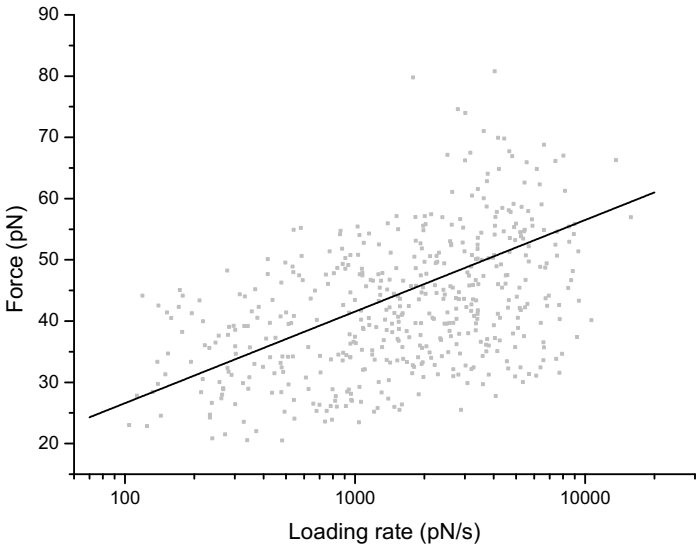

Supplementary Figure S2. SVFS dynamic force spectra of H7N9 AH1 interacting with single receptors on living MDCK cells. Scatter plot showing unbinding force *F* plotted against the loading rate r of every individual force curve. From those data, the values for k_{off} and x_u were determined to be 0.256 +/- 0.00169 s^{-1} and 6.160 +/- 0.0146 Å, respectively.

New Analysis, MLE from F vs. LR scatter plots, 2017

Virus	Cell	k_off (1/s)		x_beta (A)		tau (s)	
H1N1_WSN	A549	0.851	0.0525	2.67	0.0445	1.1751	0.0725
H1N1_WSN	CHO	0.62	0.0355	2.77	0.0397	1.6129	0.0924
H3N2_X31	A549	1.27	0.0704	6.42	0.0897	0.7874	0.0436
H3N2_X31	CHO	0.66	0.0472	9.54	0.183	1.5152	0.1084
H3N2_X31	MDCK	1.61	0.141	9.11	0.198	0.6211	0.0544

Old Analysis, fit with grouped loading rates, 2012

Virus	Cell	k_off (1/s)		x_beta (A)		tau (s)	
H1N1_WSN	A549	1.22	0.32	1.8	0.3	0.8197	0.2150
H1N1_WSN	CHO	1.16	0.13	2.4	0.3	0.8621	0.0966
H3N2_X31	A549	0.64	0.52	4.2	4.1	1.5625	1.2695
H3N2_X31	CHO	0.18	0.17	26.1	31.1	5.5556	5.2469
H3N2_X31	MDCK	0.45	0.35	8.4	7.9	2.2222	1.7284

Supplementary Table S1. Comparing SVFS results obtained using two different fitting approaches. Loading rates *LR* can either be obtained by using the mean effective spring constant $<k_{eff}>$ for each pulling velocity v ($LR = v*k_{eff}$) or, using a more adapted approach reported previously and now used in this study, calculated for each individual force-distance curve. Each fitting approach results in slightly different fitting parameters. Dissociation rate k_{off}, separation from the energy barrier x_u, and average bond lifetime τ_{off} obtained by fitting the SVFS data to a single energy barrier binding model.